Clean Block Copolymer Microparticles from Supercritical CO_2: Universal Templates for the Facile and Scalable Fabrication of Hierarchical Mesostructured Metal Oxides

Thomas M. Bennett,[a] Guping He,[a] Ryan R. Larder,[a] Michael G. Fischer,[b] Graham A. Rance,[a,c] Michael W. Fay,[c] Amanda K. Pearce,[d] Christopher D. J. Parmenter,[c] Ullrich Steiner,[b] Steven M. Howdle*[a]

[a]School of Chemistry, The University of Nottingham, University Park, Nottingham, NG7 2RD, United Kingdom

[b]Adolphe Merkle Institute, Université de Fribourg, Chemin des Verdiers 4, 1700 Fribourg, Switzerland

[c]Nanoscale and Microscale Research Centre (nmRC), The University of Nottingham, University Park, Nottingham, NG7 2RD, United Kingdom

[d]Molecular Therapeutics and Formulation Division, School of Pharmacy, University Park, Nottingham, NG7 2RD, United Kingdom

KEYWORDS: block copolymer, sol−gel, metal oxide, microparticle, mesostructured, hierarchical

ABSTRACT: Metal oxide microparticles with well-defined internal mesostructures are promising materials for a variety of different applications, but practical routes to such materials that allow the constituent structural length scales to be precisely tuned have thus far been difficult to realize. Herein, we describe a novel platform methodology that utilizes self-assembled block copolymer (BCP) microparticles synthesized by dispersion polymerization in supercritical CO_2 ($scCO_2$) as universal structure directing agents for both hydrolytic and non-hydrolytic sol-gel routes to metal oxides. Spherically structured poly(methyl methacrylate-*block*-4-vinyl pyridine) (PMMA-*b*-P4VP) BCP microparticles are translated into a series of the corresponding organic/inorganic composites and pure inorganic derivatives with a high degree of fidelity for the metal oxides TiO_2 and $LiFePO_4$. The final products are comprised of particles close to 1 μm in size with a highly ordered internal morphology of interconnected spheres between 20 – 40 nm in size. Furthermore, our approach is readily scalable, enabling grams of pure or carbon coated TiO_2 and $LiFePO_4$, respectively, to be fabricated in a facile two step route involving ambient temperature mixing and drying stages. Given that both length scales within these BCP microparticles can be controlled independently by minor variations in the reagent quantities used, the present general strategy could represent a milestone in the design and synthesis of hierarchical metal oxides with completely tunable dimensions.

The broad class of materials referred to as metal oxides possess attractive properties that make them suitable for use in a variety of applications, including catalysis,[1, 2] solar cells,[3] energy storage,[4, 5] photonics[6] and gas sensing,[7] among others. Such applications benefit from elaborate morphologies that offer dramatically increased storage, diffusion, reactivity and cycling properties as a result of their high surface-to-volume ratios. Consequently, hierarchically structured metal oxides with well-defined and repeating structures on the either the micron and/or nano scale are currently the subject of intense scientific investigation.[8-11]

Of the approaches explored to date, soft templating, hard templating and hydro/solvo-thermal routes have received the most interest, each of which typically direct the condensation of hydrolytic or non-hydrolytic sol gel precursors (or combinations thereof) to achieve the final hierarchical material. Hydro and solvothermal synthesis methods present an effective approach that affords morphological control, as demonstrated by the fabrication of diverse morphologies with short diffusion distances, such as nanoparticles,[12, 13] porous microspheres,[14-16] submicrometer-sized hollow particles,[17, 18] and nanowires.[19] However, the hydrothermal templated synthesis does have drawbacks, namely that the reaction mechanism is not easily studied and control of the size and morphology of the templated materials is usually poor and more restricted in comparison to the alternatives.[20] Furthermore, when used alone, low temperature hydrothermal methods have a tendency to form defects in the crystal structure, which can adversely affect the functional performance of the final material.[21]

The hard templating method, while proven to be an effective method for the fabrication of elaborate and well defined ordered mesoporous materials, tends to suffer in terms of practicality and scalability due to tedious multi-step procedures and the sacrifice of costly hard templates.[22] Furthermore, the obtained replicas have limited pore sizes due to the limited pore wall thicknesses (usually less than 10 nm).[9, 23, 24] By contrast, the soft templating approach is more versatile, flexible and is promising for large scale synthesis. More importantly, through this approach the mesopore structure, shape, and pore size can be easily adjusted by controlling the synthesis conditions and the properties of the template molecules.[8, 22, 25, 26]

Soft templating routes employing the Pluronic block copolymers (BCPs) have proven to be particularly popular of late due to their commercial availability, and have enabled the synthesis of a range of ordered mesoporous materials with high surface area, diverse compositions, variable pore structures and tunable

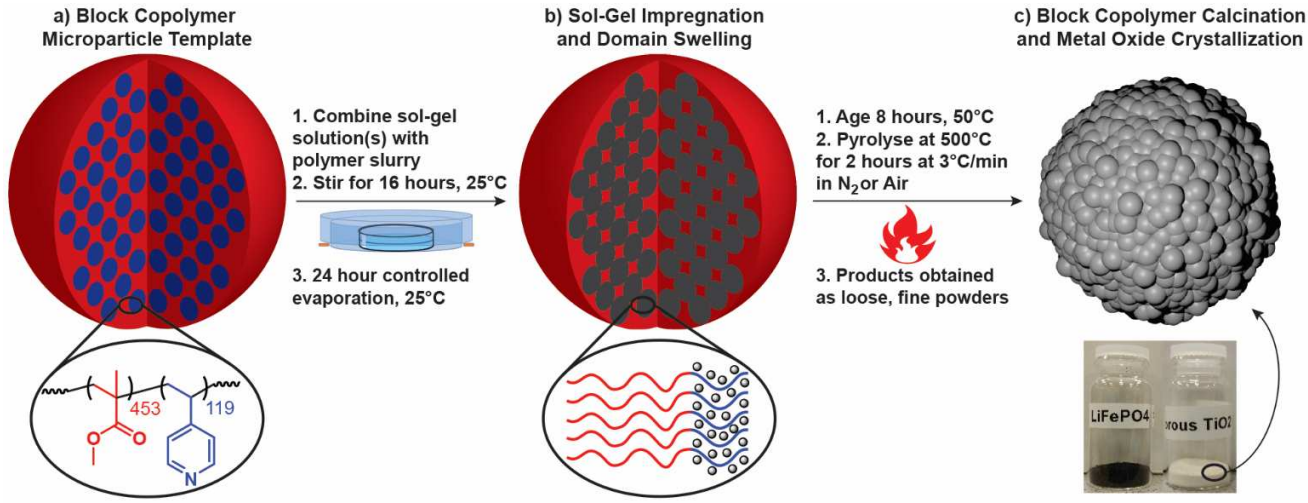

Figure 1. Illustration of the BCP microparticle sol-gel templating and calcination process. (a) The BCP microparticle template with an internal morphology of P4VP spheres surrounded by a PMMA matrix. (b) P4VP domain swelling in ethanol and simultaneous sol-gel impregnation. (c) BCP template removal and metal oxide crystallization via calcination at 500 °C in either air or N_2.

pore sizes.[5, 25, 27] However, these systems do come with their own set of limitations, largely stemming from their restrictive block chemistry, compositions, molecular weights, high oxygen content (in some cases) and lower glass transition temperatures (T_gs) than their non-Pluronic counterparts. Recent advances in the controlled radical synthesis of BCPs (via reversible addition−fragmentation chain-transfer (RAFT) polymerization, etc.) mean that bespoke BCPs can now be readily created in the laboratory through relatively facile and cheap routes.[28] Therefore, the compositions and volume fractions of each constituent block, in conjunction with the molecular weight, can be easily controlled. Thus, designing non-Pluronic amphiphilic BCPs is promising in the template directed synthesis of various mesoporous materials with controllable pore size, pore symmetry, pore wall thickness and diverse compositions.[22, 26]

Recently, our group has developed a facile, one-pot, solvent-free method for the preparation of nanostructured BCP microparticles by sequential RAFT-controlled dispersion polymerization in supercritical carbon dioxide.[29] Such microparticles were shown to be structurally diverse, and changes in the internal morphology could be introduced simply by manipulating the copolymer composition and/or chemical structure. In addition, we have also demonstrated that the overall microparticle sizes achievable using dispersion polymerization can be varied over a considerably large size range by incorporating different quantities of PDMS stabilizer before and/or during the polymerisation.[30] Critically, we have now discovered that amphiphilic derivatives of these materials can be converted into highly porous hierarchical materials through a simple swelling/deswelling approach in ethanol followed by hexane, and that the pore sizes and shapes can be readily tuned by changing the composition and molecular weight of the BCP.[31]

Following these discoveries, we hypothesized that such materials would serve as effective soft templates to direct the sol-gel synthesis of hierarchical metal oxide materials with independently controllable length scales. To this end, this article describes the sol-gel templating of a poly(methyl methacrylate-*block*-4-vinyl pyridine) (PMMA-*b*-P4VP) BCP template, towards the development of a facile and scalable platform methodology that can be readily applied to a broad range of metal oxides materials (Figure 1). P4VP is a well-known hydrophilic block that has previously been used to successfully direct the formation of simple metal oxides in films and 3D BCP materials to form elaborate morphologies, albeit at extremely low concentrations.[26, 32]

In this study, two metal oxide systems were chosen: titanium dioxide (TiO_2), which is used in an enormous number of applications ranging from pigments to photocatalysis, photovoltaics and electrical energy storage,[33] and $LiFePO_4$, a more specialized class of material that has become prominent as a cathode material in lithium-ion batteries.[34] Importantly, titanium dioxide is typically prepared via a hydrolytic route involving alkoxides,[35] whereas $LiFePO_4$ preparation is a non-hydrolytic process involving the combination of metal salts,[36] thereby highlighting the versatility of our approach.

The PMMA-*b*-P4VP BCP template employed was synthesized via RAFT dispersion polymerization in $scCO_2$ as described previously, and was obtained directly from the autoclave as a dry, free-flowing off-white powder. It will be referred to throughout the text as PMMA-4VP(45.3–12.5), with the numbers in parentheses denoting the number-average molecular weight (M_n) of each block in kDa (as determined using a combination of ^{1}H NMR spectroscopy and gel permeation chromatography (GPC), see Figure S1, Supporting Information).[29, 31] The total molecular weight of the BCP is 57.8 kDa and the molar mass dispersity ($Đ_M$) is 1.34. This corresponds to a P4VP volume fraction of 0.22, based on a PMMA density of 1.17 g/cm^3 and a P4VP density of 1.15 g/cm^3.[37] This composition was selected based on our recently published study, which identified that P4VP weight fractions in the range of 10 – 35 wt. % give rise to a morphology of P4VP spheres within a PMMA matrix, while also retaining their microparticle structure upon mixing with a P4VP selective solvent such as ethanol.[31] Prior to templating, the as-synthesized BCP sample was first imaged by

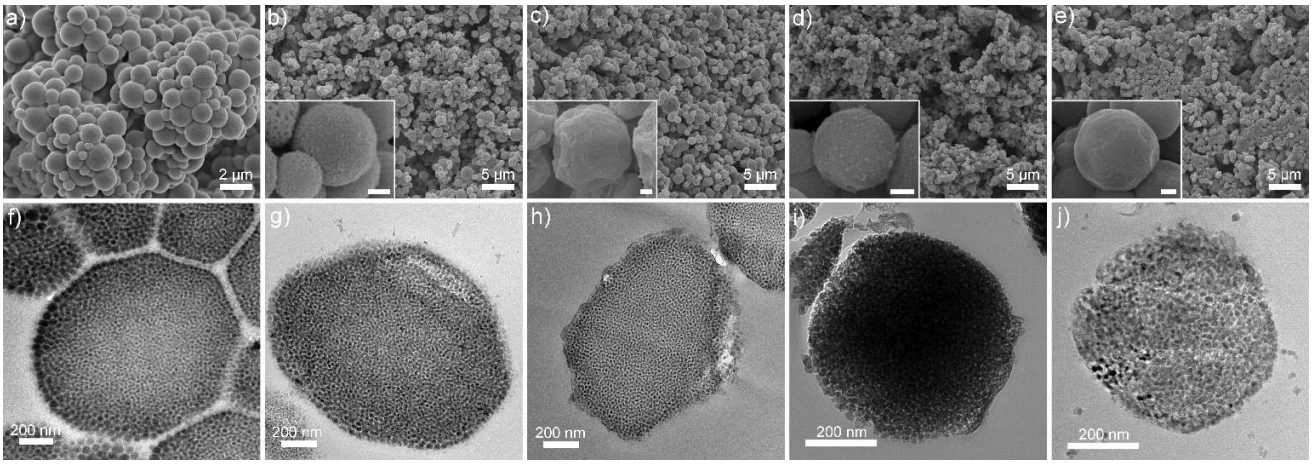

Figure 2. SEM images of the materials at each stage of the synthesis process with TEM images of the respective microparticle cross-sections underneath. (a) and (f) The BCP microparticle template. (b) and (g) The BCP/titania composite; (c) and (h) The BCP/$LiFePO_4$ composite; (d) and (i) The calcined titania microparticles; (e) and (j) The calcined $LiFePO_4$ microparticles. The P4VP domains appear dark in TEM image (f) due to iodine staining and in (g – h) due to metal oxide infusion. STEM/EDXS mapping was also used to confirm the presence of the expected elements comprising each metal oxide structure. The scale bar in the SEM inserts (not shown for clarity) is 0.2 µm.

scanning electron microscopy (SEM) and then by transmission electron microscopy (TEM) after resin embedding, ultramicrotome sectioning and iodine vapor staining. These images reveal a homogenous composition of microparticles (Figure 2a), each of which possess the expected internal morphology of PMMA matrix embedded P4VP spheres with a domain size of ~29.5 nm (dark domains due to iodine staining).

The general process developed to selectively template the BCP microparticles with either TiO_2 or $LiFePO_4$ was adapted from Fischer et al.[5, 25] and is outlined in Figure 1 (see Experimental Section for details). Briefly, it begins by mixing an ethanol solution of the appropriate sol-gel precursors with a second stock solution of a PMMA-4VP(45.3–12.5) slurry in ethanol, and allowing the resulting opaque mixture to stir at ambient temperature overnight (Figure 1a). For the TiO_2 templating we utilize an acid-stabilized sol-gel process to delay condensation, whereas the $LiFePO_4$ is formed from salts of the requisite ions (Li^+, Fe^{3+}, PO_4^{3-}). In this way, grams of material could be produced within two days once the polymer template was synthesized, simply scaling up the glassware dimensions and quantities of stock solutions proportionally, or by using the stock solutions to perform numerous templating reactions in parallel and combining the resulting products. For example, during the course of this study we have successfully scaled up our original 50 mg reactions and demonstrated that the whole process can be achieved on the 20-fold scale, yielding several hundred milligrams of metal oxide microparticles with no significant procedural changes or apparent differences in sample characteristics or morphology. Further details of these scaled up reactions can be found in the Supporting Information (also see Figure S2, Supporting Information for photographs taken during this process).

To successfully replicate the template a final P4VP:metal oxide weight ratio of ~1:1 was found to be the most suitable, with lower or higher quantities of metal oxide leading to structural collapse or microparticle fusion, respectively, during calcination. Upon contact with ethanol the P4VP domains swell and exert pressure on the surrounding PMMA matrix, eventually leading to the formation of an interconnected network of spherical domains; these domains are then gradually infused with the dissolved sol-gel precursors. Controlled evaporation of this solution at ambient or slightly elevated temperatures produces self-assembled composite BCP/titania or BCP/$LiFePO_4$ microparticles as either white or tan-colored fine powders, respectively (Figure 1b). The microphase separation of the BCP confines the titania precursor to the mesostructure, while the secondary scale of the microparticles is retained courtesy of the PMMA support matrix. A similar concept has previously been applied to induce hierarchical morphologies by self-assembly processes.[22, 26, 38]

A key advantage of our process is that both lengths scales within the hierarchical BCP structure are readily tunable over an extremely large range by simply varying the conditions of the RAFT dispersion polymerization. For the microparticle diameter, this can be achieved by varying the amount of PDMS stabilizer used, whereby a size range from 0.3 – 5.3 µm has already been reported in analogous PMMA homopolymer microparticles created in our research group.[30] The quantity of methacrylate terminated poly(dimethyl siloxane) (PDMS-MA) used to stabilize the polymerization of the PMMA-4VP(45.3–12.5) template described was 10 wt. % relative to the total monomer content, which was anticipated to produce particles with a diameter on the order of 1 µm. However, given that to the best of our knowledge there are no reports in the literature on using PDMS content to vary the diameters of BCP microparticles synthesized in $scCO_2$, we have repeated the process with only 5 wt. % of stabilizer and then used the resulting materials as a second batch of templates (discussed in more detail below). In the case of the BCP domains, spherical domains ranging from ca. 12 – 200 nm have already been achieved in BPC microparticles of PMMA-*b*-P4VP by altering the molecular weight of the two blocks.[31] Furthermore, the templated synthesis of other BCP morphologies (e.g. lamellar, etc.) is also a future possibility.

SEM imaging of both BCP/metal oxide composites reveals a similar microparticle morphology to the original BCP sample (Figure 2b – c), albeit with a more textured surface structure

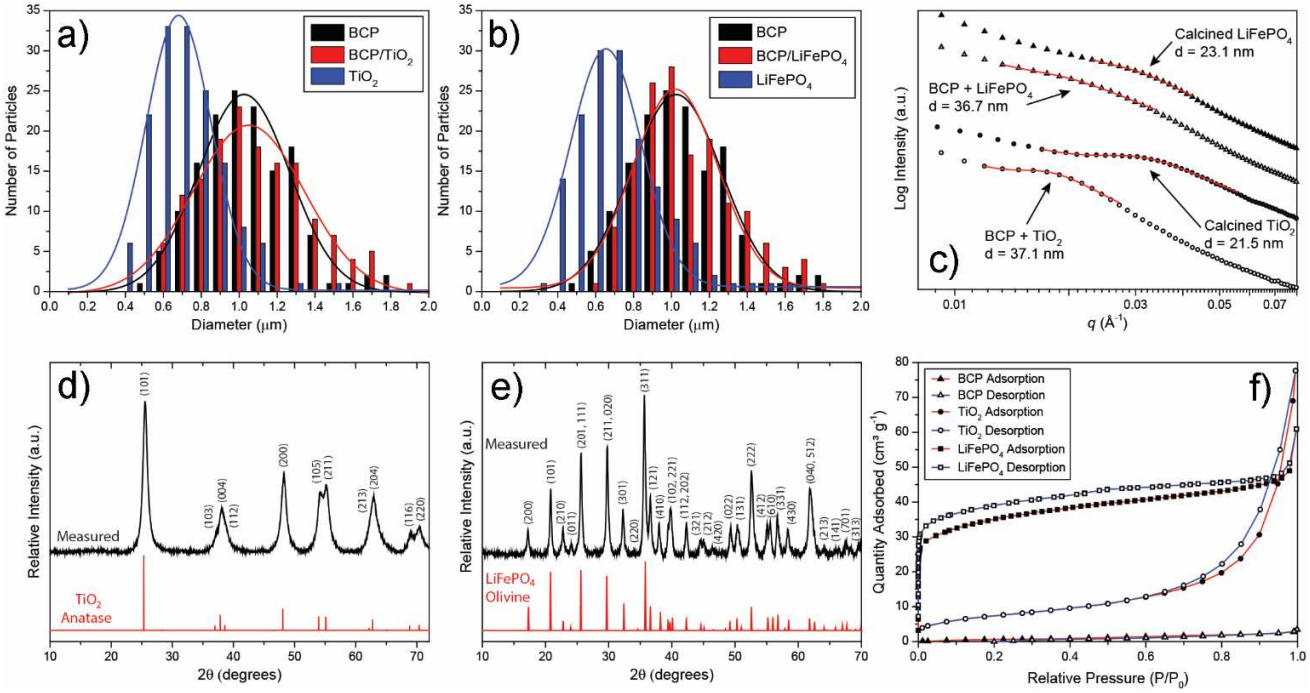

Figure 3. Characterization data from the materials at each stage of the synthesis process. (a) and (b) Microparticle size histograms obtained by measuring 150 microparticles in SEM images of the titania and $LiFePO_4$ derived materials, respectively. The lines represent Gaussian distribution fits to the data. (c) SAXS profiles of the templated materials before and after pyrolysis. The red lines are fits to the data with a combined power law Lorentzian function. (d) and (e) XRD patterns of the crystallized titania and $LiFePO_4$/carbon microparticles. (f) Physisorption isotherms for the BCP template and the crystallized titania and $LiFePO_4$/carbon microparticles.

owing to the P4VP swelling process (Figure 2b – c, inserts). Furthermore, the TEM images of the microparticles cross-sections are nearly identical to the original iodine stained BCP, thereby demonstrating that both metal oxide precursors selectively associate with the P4VP domains within the samples (Figure 2f – h). This was additionally confirmed by taking micro Raman spectra of the BCP before and after templating with TiO_2; frequency shifts of the characteristic vibrational modes of the pyridyl group after templating indicate that the titanium isopropoxide exclusively associates with the P4VP block (Figure S3, Supporting Information).

To crystallize the amorphous metal oxide precursors in the BCP composite and simultaneously remove the template, a high temperature calcination step was used (Figure 1c). When the sol-gel derived material is heated, the average grain size of the metal oxide crystallites in the mesostructured composites is controlled by the temperature.[39] This in principle allows the adjustment of the crystallite size irrespective of the pore dimensions. The minimum temperatures for calcination are given by the necessity to combust (or carbonize) all polymeric components and transform the composite into a mesoporous material. Furthermore, higher temperatures or longer annealing times are also often avoided because they can lead to a collapse of the mesopore morphology,[40, 41] particularly in titania materials where an anatase to rutile phase transition may occur.[39]

Thermogravimetric analysis (TGA) data (Figure S4a – b, Supporting Information) show that maintaining a temperature of 500 °C for two hours in either air or an inert atmosphere is needed to completely combust or carbonize the PMMA-4VP(45.3–12.5) template, respectively. As expected, the TGA trace recorded for the PMMA-4VP(45.3–12.5)/titania composite in air indicates a final titania content close to the targeted value of ~25 wt. % relative to the total content of PMMA-4VP(45.3–12.5), after subtracting the initial mass loss due to residual volatiles (Figure S4c).

For $LiFePO_4$, pyrolysis was instead performed under an inert atmosphere, due to the tendency of this material to oxidize at higher temperatures[42] and to simultaneously quantify the carbon forming potential of this BCP. The presence of a partially graphitized carbon layer is often a desirable outcome in the preparation of metal oxide phosphates for battery electrodes because it improves electrical conductivity[43, 44] and its porosity enables efficient Li^+ transport across the coating.[45] The corresponding TGA trace indicates that the remaining mass of the sample after volatile removal and BCP carbonization was 38 wt. %, due to the much greater quantity of volatiles remaining in the sample after the initial evaporation and aging steps (ascorbic acid, etc.) (Figure S4d).

To determine the amount of carbon remaining in the $LiFePO_4$/carbon composite a subsequent TGA measurement in air was performed. Taking the oxidation of $LiFePO_4$ to $Li_3Fe_2(PO_4)_3$ and Fe_2O_3 (resulting in a mass increase of 5.07 wt. %) into account,[42] the composite has a relatively high carbon content of ~30.7 wt. %, thus confirming an expected final $LiFePO_4$ content of ~25 wt. % based on the precursor quantities used (Figure S4e). Raman spectroscopy measurements were also performed to examine the molecular structure of the residual carbon coating (Figure S5, Supporting Information). The spectrum shows well pronounced peaks for the G-band (~1600 cm^{-1}) and D-band (~1350 cm^{-1}) of carbon, with a peak intensity ratio (I_D:I_G) of approximately 0.97, signifying the formation of six-fold rings and thus partial graphitization of the carbon layer.[46] The physical structure and distribution of this carbon layer is discussed in further detail below. SEM images taken following pyrolysis confirmed that the microparticle structure of the original template was retained for both samples, albeit

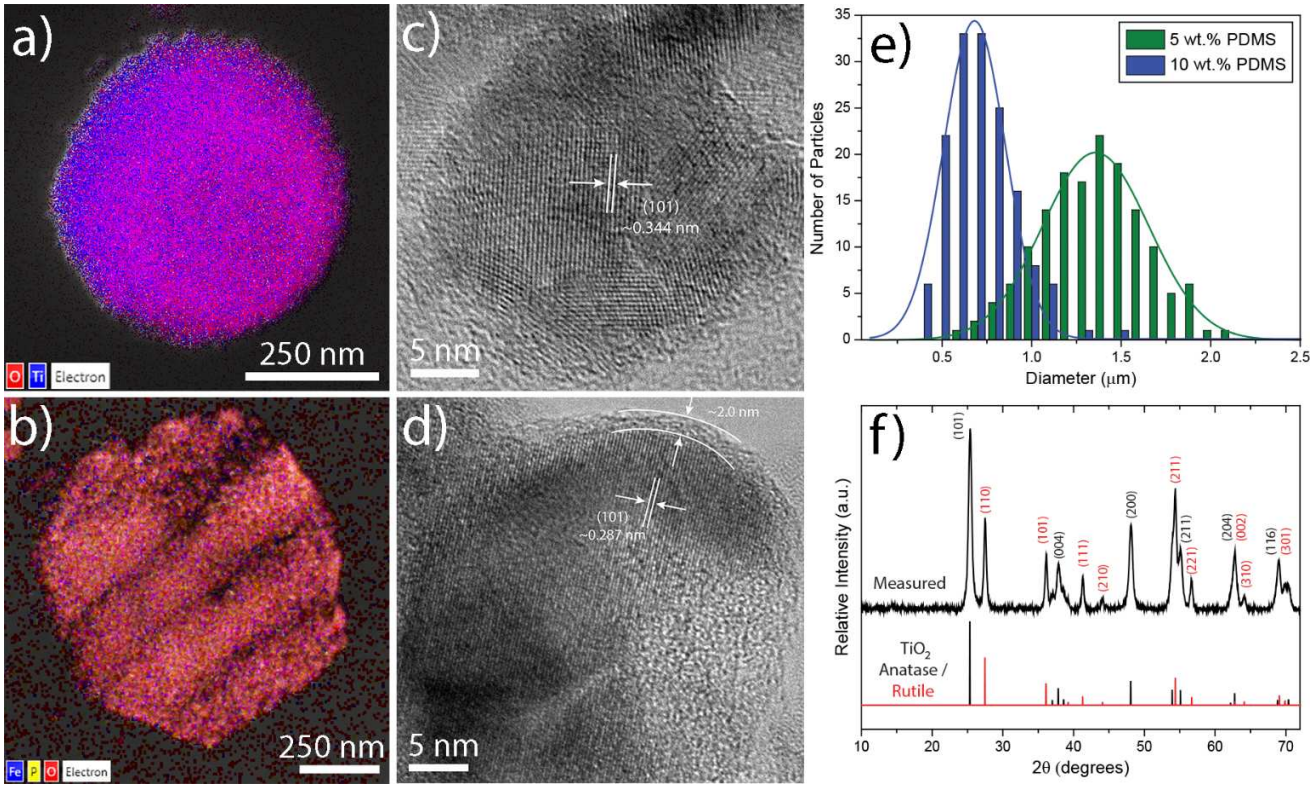

Figure 4. Additional characterization data from the BCP template derived metal oxide products. (a) and (b) Overlaid STEM/EDXS images of (a) the calcined titania microparticles and (b) the calcined $LiFePO_4$/carbon microparticles. The carbon signals have been removed for clarity. The dark lines across the microparticle are artifacts of the microtoming process. (c) and (d) High resolution FEG-TEM images of the crystallized metal oxide microparticles. (c) One domain within the crystallized titania microparticles; the spacing along the (101) direction of the anatase crystallites was measured to be approximately 0.344 nm. (d) One domain within the crystallized $LiFePO_4$/carbon microparticles; the spacing along the (101) direction of the crystallites was measured to be approximately 0.287 nm and the thickness of the surface carbon coating is approximately 2 nm. (e) Microparticle size histograms obtained by measuring 150 microparticles in SEM images of the titania materials created from BCP templates synthesized using 10 wt. % and 5 wt. % of PDMS-MA stabilizer. (f) XRD patterns of titania microparticles calcined at a higher temperature of 700 °C for 2 hours. Expected diffraction patterns of pure anatase and rutile titania are shown for reference.

with a smaller overall diameter due to the density increase upon crystallization (Figure 2d – e). To quantitatively compare the average size and size distribution of each sample, diameter measurements were taken from at least 150 microparticles for the samples before and after heat treatment (Figure 3a – b). The results are also summarized in Table 1. These data returned an average microparticle diameter of 1.12 (±0.28) μm, 1.14 (±0.30) μm and 1.16 (±0.31) μm for the as-synthesized PMMA-4VP(45.3–12.5), the titania/PMMA-4VP(45.3–12.5) composite and the $LiFePO_4$/PMMA-4VP(45.3–12.5) composite, respectively, thus indicating that no significant change in the size of the microparticles occurs during the templating process. By contrast, the samples after treatment were both approximately 32 % smaller (0.77 (±0.18) μm and 0.76 (±0.24) μm, respectively) in diameter.

High resolution field emission gun (FEG)-SEM images were then obtained to characterize the surface of the microparticles and compare differences between the samples. From these images, the templated spherical domains that comprise the remaining microparticle structure are readily observed on the surface of the titania sample (Figure 2d, insert). By contrast, the $LiFePO_4$ sample has a slightly more smooth external appearance with small, sporadically scattered pores (Figure 2e, insert). This may be a visualization of the high carbon content present throughout the microparticles after they were coated with the thin layer of iridium required to stabilize the microparticles during the imaging process. There is also the possibility that a thin shell-like metal oxide coating formed on the microparticles during the non-hydrolytic sol-gel process.

To confirm that the metal oxide loaded spherical domains were retained following crystallization, the samples were embedded in a hard epoxy resin and microtomed into thin sections (~80 nm) to allow imaging of the interior morphology by TEM (Figure 2i – j). A homogeneous, interconnected mesostructure can be observed throughout the entirety of both metal oxide microparticle samples, demonstrating that the spheres possess a high level of internal and external structural hierarchy. In addition, scanning transmission electron microscopy/energy-dispersive X-ray spectroscopy (STEM/EDXS) maps of a single microparticle from each sample serve to further corroborate that the internal domains were templated with the expected metal oxide material (Figure 4a and 4b).

SAXS data were acquired from each sample both before and after heat treatment to determine the domain size of the internal spherical morphology using the relationship $d = 2\pi/q^*$ (Figure 3c). In each case (with the exception of the pure BCP due to insufficient contrast between the two phases) a single broad peak was observed, thus corroborating our TEM observations that the morphology is persistent throughout the sample. The absence of sharper and higher order peaks signifies a lack of

long-range order, as is typically observed for BCP microparticles and short-range-ordered wormlike mesostructures.[25, 29, 38] After pyrolysis, the positional changes in these reflections from 37.1 nm to 21.5 nm and 36.7 nm to 23.1 nm for the titania and $LiFePO_4$ samples indicate that the spherical domains contract in size by approximately 42 % and 37 %, respectively (see Table 1). These reductions are slightly larger than the overall relative decrease in the average microparticle diameters for the same samples, meaning that the voids between the spherical domains recede more slowly during crystallization, possibly due to steric hindrance from the PMMA matrix as it gradually degrades. We also note that the domain sizes of the BCP/metal oxide composites is larger than those measured for the pure BCP domains in the TEM images (29.5 nm), confirming that the domains swell during the templating process in ethanol.

Table 1. Morphological Characteristics of Each Sample.

Sample	Average Microparticle Diameter (μm)	Domain Size (SAXS) (nm)	Specific Surface Area (BET) (m^2/g)	Average Pore Size (BJH) (nm)
BCP	1.12	29.5[a]	2.8	5.8
BCP/TiO_2	1.14	37.1	--	--
TiO_2	0.77	21.5	26.4	17.9
BCP/$LiFePO_4$	1.16	36.7	--	--
$LiFePO_4$/Carbon	0.76	23.1	123.0	7.8

[a]From TEM.

The porous structure and surface area of the titania and $LiFePO_4$/carbon microparticle samples were studied by N_2-adsorption measurements and the data are summarized in Table 1. As shown in Figure 3f, the N_2 adsorption-desorption isotherm for the titania sample is characteristic of type-IV with a type H1-type hysteresis loop observed in the range 0.8 – 1.0 P/P_0, indicating the presence of a mesoporous/macroporous structure. The corresponding Barrett−Joyner−Halenda (BJH) pore-size distribution (Figure S6a, Supporting Information) derived from the N_2 desorption isotherm shows a distribution of pores ranging from approximately 5 – 25 nm. In contrast, the isotherm for the $LiFePO_4$/carbon sample is typical of type-II with a H4-type hysteresis loop, and the Brunauer−Emmett−Teller (BET) surface area is considerably higher (123.0 m^2/g versus 26.4 m^2/g). This is attributed to the large quantity of microporous carbon present within the pores of this sample, which agrees with the pore-size distribution plot being dominated by pores in the range of 2 – 5 nm (Figure S6b). We emphasize here that the broadness in the pore size distributions of these materials are comparable with those reported in other recent studies involving mesoporous particles produced using soft-templating approaches with BCPs.[25, 47, 48] Furthermore, the particle size distribution data are also comparable with, or in some cases narrower than, those reported in the same studies. The reader is also referred to several recent reviews of these materials for a comparison of the characteristics and resulting functional properties achieved in materials synthesized via soft and hard templating approaches to date.[4, 22, 27, 33, 49]

The X-ray diffraction (XRD) data in Figure 3d – e confirm the respective formation of pure anatase and olivine phases for the titania and $LiFePO_4$ materials during annealing, as expected from the calcination temperatures used, with average crystallite sizes of 7 nm and 27 nm (derived from the Scherrer equation) respectively.[50] This is in agreement with high-resolution FEG-TEM images, which for the titania sample show that the mesostructure is composed of multiple crystalline grains within each spherical domain (d = 21.5 nm as determined via SAXS) (Figure 4c). By contrast, the FEG-TEM images of the $LiFePO_4$ sample show that the spherical domains are each comprised of a single crystallite, thus corroborating with the XRD calculations (Figure 4d). It is also revealed that each $LiFePO_4$ crystallite is uniformly covered with 3 – 4 layers of partially graphitized amorphous carbon that is ~2 nm in thickness. Conformal carbon coatings of comparable structure and thickness have been previously observed to form *in situ* in $LiFePO_4$ materials with polymer directed morphologies.[5, 25] This is an added cachet of soft-templating approaches because improved conductivities and Li^+ transport kinetics have been demonstrated in $LiFePO_4$/carbon materials derived in this way, as compared with those that combine $LiFePO_4$ nanoparticles with tailored (porous) carbon materials in a separate step.[5, 42, 51]

To further demonstrate the tunability of our materials and robustness of our approach, a second polymer template was fabricated in which the PDMS-MA stabilizer content was halved to 5 wt. % relative to monomer. This was done with the intention of producing BCP microparticles with an estimated average diameter approximately two fold greater (~2 um) than those discussed above (synthesized with 10 wt. % PDMS-MA), to meet future application needs where the ability to control the microparticle dimensions could lead to improved material performance. SEM images and microparticle measurements taken from the resulting polymer powder reveal that the average microparticle diameter was significantly increased to 1.94 (±0.39) μm (Figure S7a, S7b and S8, Supporting Information).

The same templating process with TTIP was then used to convert this BCP into the corresponding organic/inorganic hybrid material, which was calcined to produce the pure TiO_2 microparticles. As was observed for the template synthesised with 10 wt. % PDMS-MA, infusion of the TTIP precursor did not significantly change the microparticle diameter relative to the original BCP template, with a measured value of 1.98 (±0.44) μm. This sample also behaved in the same way as the TTIP infused template synthesised with 10 wt. % PDMS-MA upon calcination, reducing in diameter by ~31 % compared to the original BCP template (synthesised with 5 wt. % PDMS-MA), thus giving a final average diameter of 1.37 (±0.29) μm. Critically, the final TiO_2 derived microparticles using 5 wt. % PDMS-MA therefore remained close to 2 fold larger (1.78 fold) than the equivalent microparticles obtained using the BCP template fabricated with 10 wt. % PDMS-MA (Figure 4e), highlighting the ease with which the microparticle dimensions can be varied without a visible loss of the internal mesostructure (Figure S7c and S7d).

Another important factor when investigating mesostructured materials is the interplay between the key targets of a small average grain size and a high level of crystallinity. Furthermore, many applications utilizing transition metal oxides require specific crystal structures to achieve certain electronic or catalytic properties.[52] Given the broad intended applicability of the materials synthesised using this templating process, we have explored the effects of calcination temperature on the overall mesostructure and crystallite sizes in both the titania and $LiFePO_4$ products. Previous studies have shown that higher calcination temperatures and longer annealing times typically result in higher degrees of crystallinity[53-55] and better electronic conductivities of the materials.[39] The drawback is that crystal growth and coalescence during annealing can lead to a collapse of the mesopore morphology, especially in materials with small

pores. These factors have often made the simultaneous achievement of high crystallinity and structural integrity a considerable challenge in bulk and thin film titania materials templated from Pluronic BCPs.[56]

Based on previous reports that the mesostructure of soft templated materials degrades rapidly above temperatures of 700 °C,[39, 41] we have worked at 700 °C to study the effects of a higher temperature calcination process on the microparticle structure and internal morphology of each material. We also note that this temperature coincides with the reported onset of the anatase to rutile phase transition in several studies of mesoporous titania materials derived from other reported BCP templates.[39, 41] SEM images of the resulting calcined products indicate that for both of our systems the microparticle structure is not visibly altered in comparison to the samples that were calcined at the lower temperature of 500 °C (Figure S9a and S9b, Supporting Information). This was also found to be the case for the internal mesostructures, as determined from TEM images taken of microtomed cross-sections of each sample (Figure S9c and S9d, Supporting Information).

The effect of the higher 700 °C calcination temperature on the crystallite size in the two materials was evaluated by taking XRD patterns. For the titania sample this revealed that there was significant conversion of the pure anatase phase observed in the sample calcined at 500 °C into the rutile phase (Figure 4f). A sample composition of 61 wt. % rutile was subsequently calculated based on the intensities of the anatase (101) peak and the rutile (110) peak at 27.3°. The resulting anatase crystallite size by Scherrer analysis of the (101) peak gave a value of 15.4 nm, more than 2 fold larger than for the sample calcined at 500 °C. Furthermore, the rutile crystallites returned an even larger value of 20.3 nm from the (110) peak, approaching the size of the internal mesostructure as determined from the SAXS data. This may suggest that the sample was approaching the onset of mesostructure collapse caused by domain coalescence as a result of further crystallite growth at this temperature. By contrast, Scherrer analysis of the XRD data taken from the $LiFePO_4$ material (Figure S10) returned a crystallite size of 28 nm that was almost identical to that for the sample calcined at 500 °C. We attribute the lack of further crystallite growth in this material to spatial confinement by the residual carbon matrix, which has been shown previously to result in smaller crystallite sizes.[57]

In summary, we have demonstrated that nanostructured PMMA-*b*-P4VP BCP microparticles synthesized via RAFT polymerization in $scCO_2$ are versatile precursors to hierarchically structured metal oxides. Utilizing directed templating, the initial self-assembled spherical morphology of the microparticles can be translated into the corresponding inorganic/organic composites or pure inorganic derivatives with a high degree of fidelity. The key advantages of our approach over other current routes are: (1) The templates themselves are created using a solvent free process from relatively cheap precursors, and as we have demonstrated previously, the two primary length scales (nano and micro) comprising the hierarchical structure can both be independently tuned over an extremely wide range. Specifically, microparticle diameters between 0.3 – 5.3 μm and spherical domain sizes of 12 – 60 nm have already been demonstrated in comparable materials, simply through minor variations in the polymerization reaction. We then further validated these claims by increasing the size of the pure titania microparticles by templating them from a second batch of polymer synthesized using half the quantity of PDMS-MA stabilizer originally investigated (5 wt. % instead of 10 wt. % of the total monomer content). (2) The entire process is readily scalable. A single polymerization produces ~10 grams of readily templatable BCP and further increases beyond this point are not anticipated to be overly problematic, simply requiring the development of larger reaction vessels. We have also demonstrated here that the templating process itself is high throughput, having successfully produced grams of both pure and carbon containing mesostructured metal oxide microparticles. (3) Our synthesis protocol works equally effectively for both of the hydrolytic and non-hydrolytic sol-gel reaction mechanisms investigated so far, thus establishing itself as a candidate platform technology that can likely be adapted directly to a range of other systems. (4) The microparticles and mesostructures comprising both materials are stable for > 2 hours at calcination temperatures of 700 °C. Varying the calcination temperature was also shown to be suitable for controlling the crystallite size and proportion of the anatase and rutile phases in the titania products. (5) The BCP template can be readily exploited as a convenient source of amorphous carbon that effectively coats the internal spherical domains, simply by pyrolyzing the sample under inert gas. Further systematic studies, including the ability to successfully replicate different BCP morphologies (e.g. lamellae, etc.) with several metal oxide materials, will be the scope of future work.

EXPERIMENTAL SECTION

Polymer Synthesis and Characterization. The BCP microparticle sample used in this study was synthesized using RAFT dispersion with the RAFT agent 2-(dodecylthiocarbonothioylthio)-2-methylpropionic acid) trithiocarbonate (DDMAT) according to literature procedures.[29, 31] DDMAT was synthesized as described previously.[58] Unless stated otherwise, all chemicals were purchased from Sigma Aldrich and used without further purification. To target a PMMA block length of 50 kg mol^{-1}, methyl methacrylate (7.5 g, inhibitor removed) containing 2,2'-azobis(butyronitrile) (AIBN) (25 mg), DDMAT (55 mg) and methacrylate terminated poly(dimethyl siloxane, M_n ~10 kDa) (PDMS-MA) (1.0 g or 0.5 g, as specified, Fluorochem) was degassed by bubbling with argon for 30 minutes at 0 °C before being charged into a degassed 60 mL autoclave under a positive flow of CO_2. The autoclave was then pressurized to 50 bar at room temperature before being steadily increased to the final polymerization conditions of 275 bar and 65 °C. After stirring at 300 rpm for 18 hours, a small quantity of homopolymer was collected through the outlet tap for analysis before degassed 4-vinyl pyridine (2.5 mL) containing additional AIBN (6.25 mg) was added to the autoclave at a rate of 1 mL min^{-1} using a HPLC pump (Jasco). After reacting for a further 18 hours the autoclave was cooled to 45 °C (2000 psi) and flushed with additional CO_2 (at a constant pressure) for 15 minutes to remove any residual monomer before venting. The PMMA-*b*-P4VP BCP product (8.30 g) was collected as a dry, off-white free flowing powder and characterized via ^{1}H NMR spectroscopy in $CDCl_3$ (Bruker AV3400 spectrometer, 400 MHz) and GPC (Polymer Laboratories GPC50, Agilent Mixed D columns) in DMF with 0.1 wt. % LiBr against PMMA standards at a flow rate of 1 mL min^{-1}. PMMA standards (M_n range: 500 – 1,810,000 g mol^{-1}) were used as calibrants.

Mesoporous Metal Oxide Microparticle Synthesis. The metal oxide templated BCP microparticles were synthesized by typical sol-gel procedures for TiO_2 and $LiFePO_4$, targeting a final mass of 25 wt. % metal oxide relative to BCP. The sol-gel solution for TiO_2 templating was created by adding titanium

tetraisopropoxide (TTIP) (0.062 mL) to a solution of concentrated hydrochloric acid (0.031 mL, 37 wt. % HCl in H_2O) in ethanol (8.92 mL) for a final volume of 8 mL and stirring for 60 minutes. During this time, a slurry of PMMA-*b*-P4VP in ethanol was created at a concentration of 25 mg/mL by continuous stirring at 1000 rpm to yield a stock mixture. 2 mL of this PMMA-*b*-P4VP solution was then combined with the sol-gel mixture and stirred overnight at 500 rpm, before being evaporated in a small Petri dish (5 cm diameter) placed inside a larger enclosed Petri dish (12 cm diameter) separated with thin spacers (~0.1 cm in height) for 24 hours at room temperature (22 °C). Each sample was further dried in an oven at 50 °C for 8 hours and obtained as a fine white powder (77 mg) that was loosely settled on the dish surface. This drying step is largely superfluous to the fabrication of the pure metal oxide samples, and only necessary if a fully dry BCP/metal oxide composite is desired quickly. The $LiFePO_4$ templated materials were created in a similar fashion, with the exception that the sol-gel solution was created by combining solutions of FeCl(III) (0.110 mL of a 1 M ethanol solution), ascorbic acid (0.291 mL of a 1 M H_2O solution), LiCl (0.113 mL of a 1 M 75/25 wt. % ethanol/H_2O solution) and phosphoric acid (0.0162 mL of a 50 wt. % H_2O solution) in ethanol (7.47 mL). A molar excess of approximately 3 % lithium was used to ensure phase purity. The product was obtained as a fine amber colored powder (105 mg) that was loosely settled on the dish surface. The TiO_2 and $LiFePO_4$ products were calcined in a tube furnace at 500 °C (or 700 °C where specified) for 2 hours (3 °C min^{-1} ramp) in air or under a flow of N_2, respectively, and obtained as either fine white (19 mg) or black powders (39 mg).

Polymer and Metal Oxide Microparticle Characterization. The microstructure of the polymer and metal oxide samples was imaged with a JEOL 7100F FEG-SEM, after first being coated with a 10 nm layer of iridium. The internal mesostructures were imaged using a JEOL 2100Plus TEM with a LaB_6 source operating at an accelerating voltage of 200 kV (80 kV for the pure BCP) equipped with a Gatan US1000 camera. STEM/EDXS maps of the sample elemental composition were acquired during the imaging process using an Oxford Instruments XMax 100TLE detector controlled through the Aztec software package. High-resolution FEG-TEM images were collected using a JEOL 2100F FEG-TEM operating at an accelerating voltage of 200 kV in conjunction with a Gatan Orius SC100 camera. In all cases, the samples for TEM imaging were first set in Agar 100 resin at 50 °C for 48 hours before being sliced into ~80 nm sections using a Diatome diamond knife attached to an RMC Powertome ultramicrotome. Where stated, the BCP sections were then stained with iodine vapor for 2 hours prior to imaging. XRD patterns were obtained from a PANanalytical X'Pert³ diffractometer over a 2θ range from 10° to 70° using a Cu Kα radiation source (λ = 0.15406 nm). Physisorption measurements for the calculation of specific surface areas (BET) and pore size distributions (BJH) were conducted at 77 K with a Micromeritics 3Flex Surface Area Analyzer using N_2 as the adsorbate. The BCP and metal oxide samples were first degassed at 50 °C and 150 °C, respectively, for 16 hours prior to measuring. The characteristic period of the mesostructure was determined via SAXS using a Rigaku NanoMAX-IQ™ camera equipped with a Cu target sealed tube source (MicroMax 003™ microfocus from Rigaku). The scattering data were collected using a Pilatus100K detector (Dectris). The sample-to-detector distance was calibrated using a silver behenate standard. TGA was performed with a TA Instruments Discovery™ system using platinum crucibles and a temperature range of 30 °C to 500 °C with a heating rate of 3 °C min^{-1} in N_2 or air, as appropriate. ^{1}H NMR spectra were recorded on a Bruker 400 MHz spectrometer using chloroform-d_3 as the solvent. Micro Raman spectroscopy was performed using a Horiba Jobin Yvon LabRAM HR Raman spectrometer. Spectra were acquired using a Synapse CCD detector (1024 pixels) thermoelectrically cooled to −60 °C. Before spectra collection, the instrument was calibrated using the zero-order line and a standard Si(100) reference band at 520.7 cm^{-1}.

ASSOCIATED CONTENT

Supporting Information

The Supporting Information is available free of charge on the ACS Publications website at DOI: XXX.

^{1}H NMR and GPC characterization data for the BCP template; Photographs of the scaled up templating reactions; TGA measurements of the BCP, the BCP/metal oxide composites and the pyrolyzed $LiFePO_4$/carbon product in air and/or N_2; Raman data from the pyrolyzed $LiFePO_4$/carbon product; pore size distribution data; SEM and TEM images and particle size histograms of the BCP template prepared using 5 wt. % PDMS-MA stabilizer and the corresponding titania microparticles; SEM and TEM images of the titania and $LiFePO_4$/carbon microparticles calcined at 700 °C; XRD data for the $LiFePO_4$/carbon microparticles calcined at 700 °C.

AUTHOR INFORMATION

Corresponding Author

*Email: steve.howdle@nottingham.ac.uk

Author Contributions

The manuscript was written through contributions of all authors. All authors have given approval to the final version of the manuscript.

Funding Sources

Leverhulme Trust (RPG-2014-034). Engineering and Physical Sciences Research Council (EPSRC) (EP/L022494/1).

Notes

The authors declare no competing financial interest.

ORCID

Thomas M. Bennett: 0000-0002-6388-3424

Ryan R. Larder: 0000-0002-3412-2570

Michael G. Fischer: 0000-0002-0519-5463

Graham A. Rance: 0000-0002-8325-1096

Michael W. Fay: 0000-0003-0017-5196

Amanda K. Pearce: 0000-0003-3372-7380

Ullrich Steiner: 0000-0001-5936-339X

Steven M. Howdle: 0000-0001-5901-8342

ACKNOWLEDGEMENT

We are grateful to the Leverhulme Trust (RPG-2014-034) for their support of this project (TMB, GH and SMH). The election microscope instruments used for this work are supported by the Engineering and Physical Sciences Research Council (EPSRC) (EP/L022494/1) and the University of Nottingham. The authors thank the Nanoscale and Microscale Research Centre (nmRC) for providing access to instrumentation. We also acknowledge the technical assistance provided by Dr. Elisabeth Steer and Miss. Alison Taylor, in addition to the invaluable technical support received from our high pressure workshop technicians Mr.

Richard Wilson and Mr. Peter Fields. We thank Prof. Andrei Khlobystov and his research group for access to their equipment. MGF and US acknowledge funding from the Swiss National Science Foundation through the NRP70 (153764) program and from the Adolphe Merkle Foundation. Finally, we thank Dr. Xiao Hua and Dr. Ilja Gunkel for insightful discussions.

REFERENCES

1. Parlett, C. M. A.; Wilson, K.; Lee, A. F., *Chem. Soc. Rev.* **2013,** 42, 3876-3893.
2. Zhu, C.; Li, H.; Fu, S.; Du, D.; Lin, Y., *Chem. Soc. Rev.* **2016,** 45, 517-531.
3. Roose, B.; Gödel, K. C.; Pathak, S.; Sadhanala, A.; Baena, J. P. C.; Wilts, B. D.; Snaith, H. J.; Wiesner, U.; Grätzel, M.; Steiner, U.; Abate, A., *Adv. Energy Mater.* **2016,** 6, 1501868.
4. Li, W.; Liu, J.; Zhao, D., *Nat. Rev. Mater.* **2016,** 1, 16023.
5. Fischer, M. G.; Hua, X.; Wilts, B. D.; Castillo-Martínez, E.; Steiner, U., *ACS Appl. Mater. Interfaces* **2018,** 10, 1646-1653.
6. Shopsowitz, K. E.; Qi, H.; Hamad, W. Y.; MacLachlan, M. J., *Nature* **2010,** 468, 422.
7. Sun, Y.-F.; Liu, S.-B.; Meng, F.-L.; Liu, J.-Y.; Jin, Z.; Kong, L.-T.; Liu, J.-H., *Sensors* **2012,** 12, 2610.
8. Wang, X.; Zhang, Y.; Luo, W.; Elzatahry, A. A.; Cheng, X.; Alghamdi, A.; Abdullah, A. M.; Deng, Y.; Zhao, D., *Chem. Mater.* **2016,** 28, 2356-2362.
9. Wang, H.; Zhuo, S.; Liang, Y.; Han, X.; Zhang, B., *Angew. Chem., Int. Ed.* **2016,** 55, 9055-9059.
10. Ren, Y.; Zhou, X.; Luo, W.; Xu, P.; Zhu, Y.; Li, X.; Cheng, X.; Deng, Y.; Zhao, D., *Chem. Mater.* **2016,** 28, 7997-8005.
11. Ke, Q.; Guan, C.; Zhang, X.; Zheng, M.; Zhang, Y.-W.; Cai, Y.; Zhang, H.; Wang, J., *Adv. Mater. (Weinheim, Ger.)* **2017,** 29, 1604164.
12. Pan, A.; Wu, H. B.; Yu, L.; Lou, X. W., *Angew. Chem.* **2013,** 125, 2282-2286.
13. Ma, Z.; Shao, G.; Fan, Y.; Wang, G.; Song, J.; Liu, T., *ACS Appl. Mater. Interfaces* **2014,** 6, 9236-9244.
14. Li, J.; Xiong, S.; Liu, Y.; Ju, Z.; Qian, Y., *ACS Appl. Mater. Interfaces* **2013,** 5, 981-988.
15. Deng, Y.; Cai, Y.; Sun, Z.; Liu, J.; Liu, C.; Wei, J.; Li, W.; Liu, C.; Wang, Y.; Zhao, D., *J. Am. Chem. Soc.* **2010,** 132, 8466-8473.
16. Zhao, J.; Zou, Y.; Zou, X.; Bai, T.; Liu, Y.; Gao, R.; Wang, D.; Li, G.-D., *Nanoscale* **2014,** 6, 7255-7262.
17. Zhang, G.; Lou, X. W., *Angew. Chem.* **2014,** 126, 9187-9190.
18. Lai, X.; Li, J.; Korgel, B. A.; Dong, Z.; Li, Z.; Su, F.; Du, J.; Wang, D., *Angew. Chem.* **2011,** 123, 2790-2793.
19. Peng, L.; Zhao, Y.; Ding, Y.; Yu, G., *Chem. Commun. (Cambridge, U. K.)* **2014,** 50, 9569-9572.
20. Liu, Y.; Goebl, J.; Yin, Y., *Chem. Soc. Rev.* **2013,** 42, 2610-2653.
21. Jensen, K. M. Ø.; Christensen, M.; Gunnlaugsson, H. P.; Lock, N.; Bøjesen, E. D.; Proffen, T.; Iversen, B. B., *Chem. Mater.* **2013,** 25, 2282-2290.
22. Deng, Y.; Wei, J.; Sun, Z.; Zhao, D., *Chem. Soc. Rev.* **2013,** 42, 4054-4070.
23. Wang, J.; Yang, N.; Tang, H.; Dong, Z.; Jin, Q.; Yang, M.; Kisailus, D.; Zhao, H.; Tang, Z.; Wang, D., *Angew. Chem.* **2013,** 125, 6545-6548.
24. Xu, S.; Hessel, C. M.; Ren, H.; Yu, R.; Jin, Q.; Yang, M.; Zhao, H.; Wang, D., *Energy Environ. Sci.* **2014,** 7, 632-637.
25. Fischer, M. G.; Hua, X.; Wilts, B. D.; Gunkel, I.; Bennett, T. M.; Steiner, U., *ACS Appl. Mater. Interfaces* **2017,** 9, 22388-22397.
26. Connal, L. A.; Lynd, N. A.; Robb, M. J.; See, K. A.; Jang, S. G.; Spruell, J. M.; Hawker, C. J., *Chem. Mater.* **2012,** 24, 4036-4042.
27. Boyjoo, Y.; Wang, M.; Pareek, V. K.; Liu, J.; Jaroniec, M., *Chem. Soc. Rev.* **2016,** 45, 6013-6047.
28. Chiefari, J.; Chong, Y. K.; Ercole, F.; Krstina, J.; Jeffery, J.; Le, T. P. T.; Mayadunne, R. T. A.; Meijs, G. F.; Moad, C. L.; Moad, G.; Rizzardo, E.; Thang, S. H., *Macromolecules* **1998,** 31, 5559-5562.
29. Jennings, J.; Beija, M.; Richez, A. P.; Cooper, S. D.; Mignot, P. E.; Thurecht, K. J.; Jack, K. S.; Howdle, S. M., *J. Am. Chem. Soc.* **2012,** 134, 4772-4781.
30. McAllister, T. D.; Farrand, L. D.; Howdle, S. M., *Macromol. Chem. Phys.* **2016,** 217, 2294-2301.
31. He, G.; Bennett, T. M.; Alauhdin, M.; Fay, M. W.; Liu, X.; Schwab, S. T.; Sun, C.-g.; Howdle, S. M., *Polym. Chem.* **2018,** 9, 3808-3819.
32. Choudhury, S.; Agrawal, M.; Formanek, P.; Jehnichen, D.; Fischer, D.; Krause, B.; Albrecht, V.; Stamm, M.; Ionov, L., *ACS Nano* **2015,** 9, 6147-6157.
33. Fattakhova-Rohlfing, D.; Zaleska, A.; Bein, T., *Chem. Rev. (Washington, DC, U. S.)* **2014,** 114, 9487-9558.
34. Wang, J.; Sun, X., *Energy Environ. Sci.* **2015,** 8, 1110-1138.
35. Cargnello, M.; Gordon, T. R.; Murray, C. B., *Chem. Rev. (Washington, DC, U. S.)* **2014,** 114, 9319-9345.
36. Satyavani, T. V. S. L.; Srinivas Kumar, A.; Subba Rao, P. S. V., *Eng. Sci. Technol. Int J.* **2016,** 19, 178-188.
37. Brandrup, J.; Immergut, E. H.; Grulke, E. A., *Polymer Handbook, 4th Edition*. Wiley: 1999.
38. Kang, E.; Jung, Y. S.; Kim, G.-H.; Chun, J.; Wiesner, U.; Dillon, A. C.; Kim, J. K.; Lee, J., *Adv. Funct. Mater.* **2011,** 21, 4349-4357.
39. Guldin, S.; Huttner, S.; Tiwana, P.; Orilall, M. C.; Ulgut, B.; Stefik, M.; Docampo, P.; Kolle, M.; Divitini, G.; Ducati, C.; Redfern, S. A. T.; Snaith, H. J.; Wiesner, U.; Eder, D.; Steiner, U., *Energy Environ. Sci.* **2011,** 4, 225-233.
40. Jo, C.; Kim, Y.; Hwang, J.; Shim, J.; Chun, J.; Lee, J., *Chem. Mater.* **2014,** 26, 3508-3514.
41. Fattakhova-Rohlfing, D.; Wark, M.; Brezesinski, T.; Smarsly, B. M.; Rathouský, J., *Adv. Funct. Mater.* **2007,** 17, 123-132.
42. Yang, J.; Wang, J.; Tang, Y.; Wang, D.; Li, X.; Hu, Y.; Li, R.; Liang, G.; Sham, T.-K.; Sun, X., *Energy Environ. Sci.* **2013,** 6, 1521-1528.
43. Bruce, P. G.; Scrosati, B.; Tarascon, J.-M., *Angew. Chem., Int. Ed.* **2008,** 47, 2930-2946.
44. Song, J.; Sun, B.; Liu, H.; Ma, Z.; Chen, Z.; Shao, G.; Wang, G., *ACS Appl. Mater. Interfaces* **2016,** 8, 15225-15231.
45. Wu, X.-L.; Jiang, L.-Y.; Cao, F.-F.; Guo, Y.-G.; Wan, L.-J., *Adv. Mater. (Weinheim, Ger.)* **2009,** 21, 2710-2714.
46. Ferrari, A. C.; Robertson, J., *Phys. Rev. B* **2000,** 61, 14095-14107.
47. Wei, J.; Wang, H.; Deng, Y.; Sun, Z.; Shi, L.; Tu, B.; Luqman, M.; Zhao, D., *J. Am. Chem. Soc.* **2011,** 133, 20369-20377.
48. Yue, Q.; Wang, M.; Wei, J.; Deng, Y.; Liu, T.; Che, R.; Tu, B.; Zhao, D., *Angew. Chem., Int. Ed.* **2012,** 51, 10368-10372.
49. Lai, X.; Halpert, J. E.; Wang, D., *Energy Environ. Sci.* **2012,** 5, 5604-5618.
50. Patterson, A. L., *Phys. Rev.* **1939,** 56, 978-982.
51. Yang, J.; Wang, J.; Tang, Y.; Wang, D.; Xiao, B.; Li, X.; Li, R.; Liang, G.; Sham, T.-K.; Sun, X., *J. Mater. Chem. A* **2013,** 1, 7306-7311.
52. Dahl, M.; Liu, Y.; Yin, Y., *Chem. Rev. (Washington, DC, U. S.)* **2014,** 114, 9853-9889.
53. Rodriguez, E. F.; Chen, D.; Hollenkamp, A. F.; Cao, L.; Caruso, R. A., *Nanoscale* **2015,** 7, 17947-17956.
54. Stefik, M.; Song, J.; Sai, H.; Guldin, S.; Boldrighini, P.; Orilall, M. C.; Steiner, U.; Gruner, S. M.; Wiesner, U., *J. Mater. Chem. A* **2015,** 3, 11478-11492.
55. Wang, J.; Zhou, Y.; Hu, Y.; O'Hayre, R.; Shao, Z., *J. Phys. Chem. C* **2011,** 115, 2529-2536.
56. Zukalová, M.; Zukal, A.; Kavan, L.; Nazeeruddin, M. K.; Liska, P.; Grätzel, M., *Nano Lett.* **2005,** 5, 1789-1792.
57. Lee, J.; Christopher Orilall, M.; Warren, S. C.; Kamperman, M.; DiSalvo, F. J.; Wiesner, U., *Nat. Mater.* **2008,** 7, 222.
58. Lai, J. T.; Filla, D.; Shea, R., *Macromolecules* **2002,** 35, 6754-6756.

Table of Contents artwork:

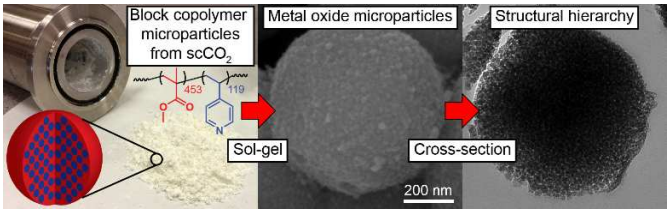
Block copolymer microparticles from scCO2
453
119
Sol-gel
Metal oxide microparticles
Cross-section
Structural hierarchy
200 nm